Photochemical & Photobiological Sciences

Accepted Manuscript

This is an *Accepted Manuscript*, which has been through the Royal Society of Chemistry peer review process and has been accepted for publication.

Accepted Manuscripts are published online shortly after acceptance, before technical editing, formatting and proof reading. Using this free service, authors can make their results available to the community, in citable form, before we publish the edited article. We will replace this *Accepted Manuscript* with the edited and formatted *Advance Article* as soon as it is available.

You can find more information about *Accepted Manuscripts* in the Information for Authors.

Please note that technical editing may introduce minor changes to the text and/or graphics, which may alter content. The journal's standard Terms & Conditions and the Ethical guidelines still apply. In no event shall the Royal Society of Chemistry be held responsible for any errors or omissions in this *Accepted Manuscript* or any consequences arising from the use of any information it contains.

ROYAL SOCIETY OF CHEMISTRY

www.rsc.org/pps

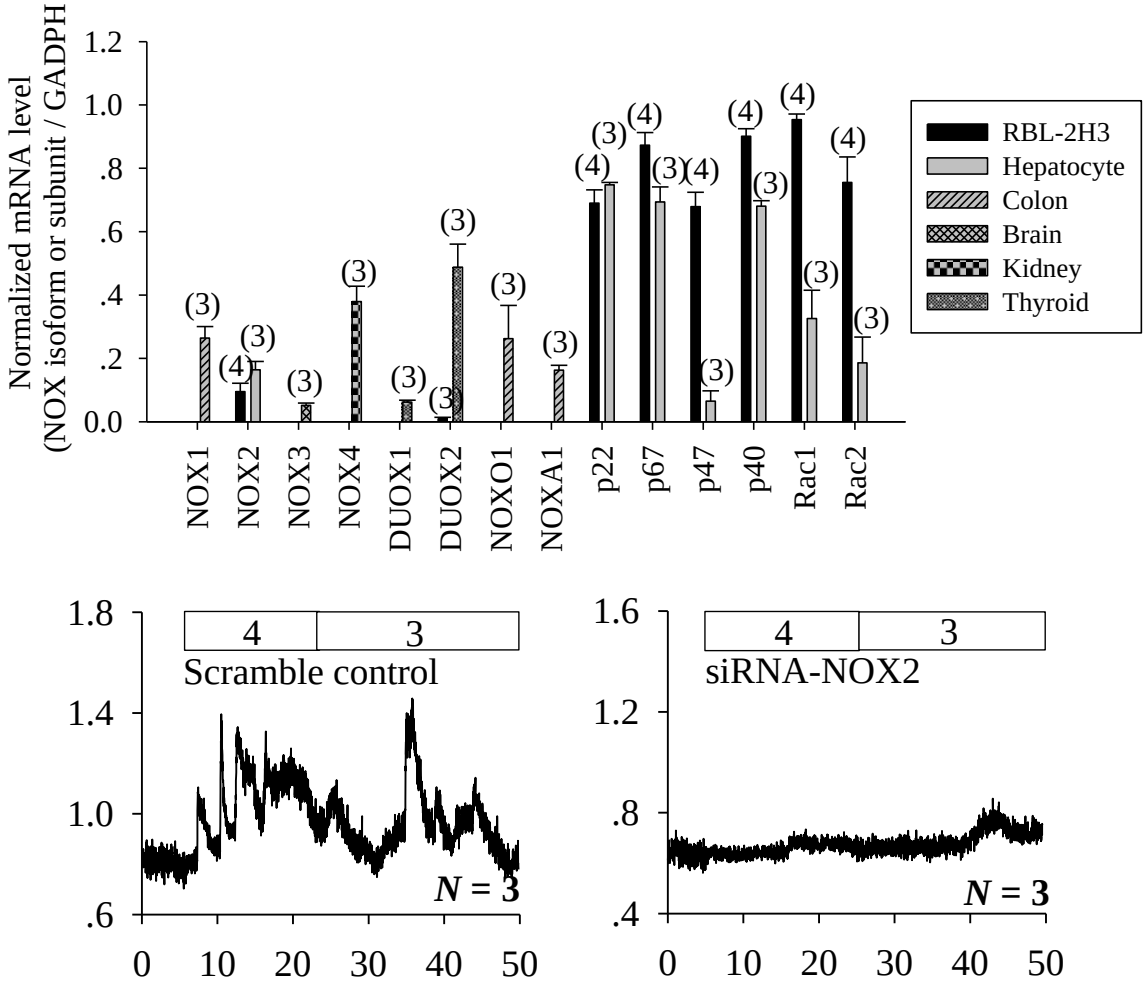

UVA irradiation triggers calcium oscillations in mast cells, which are obliterated completely after siRNA down-regulation of NOX2 and associated subunits, consistent with the fact that mast cells express predominantly NOX2.

An essential role for NAD(P)H oxidase 2 in UVA-induced calcium oscillations in mast cells

Zhi Ying Li, Zong Jie Cui*
Institute of Cell Biology, Beijing Normal University, Beijing 100875, China

Running title: NOX2 responsible for UVA-induced calcium oscillations

Please address all correspondence to:
Zong Jie Cui, Ph.D. (Cantab.),
Professor and Founding Director
Institute of Cell Biology
Beijing Normal University
Beijing 100875, China
Tel: +86 10 58809162
E-mail: zjcui@bnu.edu.cn

Abstract

Solar UVA radiation (320-400 nm) is known to have immunomodulatory effects, but the detailed mechanisms involved are not fully elucidated. UVA irradiation has been shown to induce calcium oscillations in rat peritoneal mast cells due to NAD(P)H oxidase (NOX) activation, but the specific NOX isoforms have not been identified. In the present work effects of UVA irradiation were investigated in isolated rat peritoneal mast cells, in cultured rat mast cell line RBL-2H3, and in mouse bone marrow-derived mast cells (BMMC). It was found that UVA irradiation by alternate 340/380 nm (3.2-5.6 $\mu W.cm^{-2}$) or by LED (380 nm, 80 $\mu W.cm^{-2}$) induced calcium oscillations in isolated rat peritoneal mast cells, in RBL-2H3, and in BMMC. Such UVA induced calcium oscillations resembled closely those induced by surface IgE receptor (FcεRI) activation. It was found that RBL-2H3 expressed high level $gp91^{phox}$ (NOX2), $p22^{phox}$, $p67^{phox}$, $p47^{phox}$, $p40^{phox}$, Rac1, Rac2, moderate level DUOX2, but did not express NOX1, NOX3, NOX4, or DUOX1. The specific cellular localizations of $gp91^{phox}$ (NOX2), $p22^{phox}$, $p47^{phox}$, $p67^{phox}$, $p40^{phox}$ and Rac1/2 were confirmed by immunocytochemistry. UVA-induced reactive oxygen species (ROS) production in RBL-2H3 was completely suppressed by NOX inhibitor diphenyleneiodonium (DPI) or by antioxidant N-acety-L-cysteine (NAC). siRNA suppression of $gp91^{phox}$ (NOX2), $p22^{phox}$, $p47^{phox}$ expression inhibited markedly UVA-induced calcium oscillations, ROS and IL-6 / LTC_4 production in RBL-2H3. Taken together these data indicate that NOX2 plays an essential role in UVA irradiation-induced calcium oscillations, ROS and mediator production in mast cells.

Introduction

Oscillatory increases in cytosolic calcium in different cell types including mast cells ensure that multiple and specific signals are encoded. Calcium oscillations could be induced by physiological concentrations of hormones and neurotransmitters[1-3], bacterial cytotoxin or IgE[4,5], but also by ultraviolet A irradiation (UVA, 320-400 nm)[6]. Of the solar UV radiation, only UVA and UVB (290-320 nm) can reach the surface of the earth, of which about 95% is UVA[7-9]. Therefore UVA is of particular biological significance. UVA can penetrate to skin dermis, to be absorbed by endogenous photosensitizers in dermal fibroblasts, granular leukocytes, endothelial cells and mast cells[10-12]. UVA absorption by endogenous photosensitizers riboflavin, porhyrin, flavin mononucleotide A, flavin adenine dinucleotide (FAD), β-nicotinamide adenine dinucleotide (NAD) and β-nicotinamide adenine dinucleotide phosphate (NADP) elicits photodynamic action and singlet oxygen ($^1O_2$) generation[13-17].

We recently reported that low dose (1-10 $\mu W.cm^{-2}$) UVA irradiation activates NAD(P)H oxidase (NOX), to produce reactive oxygen species (ROS), activate phospholipase C, induce calcium oscillations in rat peritoneal mast cells[6]. The facts that NOX inhibitor and antioxidant blocked completely UVA-induced ROS production and calcium oscillations, that the fluorescence emission spectrum of single mast cell displayed characteristic peaks of NAD(P)H[6,18,19], all indicated that UVA-irradiated mast cells produced ROS via NOX activation, although the NOX isoforms responsible have not been identified[6]. Here we have extended our previous work to find that UVA irradiation by both alternate UVA irradiation (340/380 nm, 3.2-5.6 $\mu W.cm^{-2}$) and by LED irradiation (380 nm, 80 $\mu W.cm^{-2}$) induced calcium oscillations not only in rat peritoneal mast cells, but also in cultured rat mast cell line RBL-2H3 and in mouse bone marrow-derived mast cells (BMMC), which all resembled closely calcium oscillations induced by IgE receptor (FceRI) activation. We present strong evidence that such UVA-induced calcium oscillations were mediated by the activation of NOX2, the isoform that all three types of mast cells predominantly expressed. The present findings may open up new avenues for NOX2-focused treatment of solar irradiation-induced skin conditions.

Material and Methods

Reagents

Anti-dinitrophenyl (anti-DNP) IgE monoclonal antibody, catalase, diphenyleneiodonium chloride (DPI) and N-acetyl-cysteine (NAC) were purchased from Sigma-Aldrich (St. Louis, MO, USA). DNP-BSA conjugate was purchased from Alpha Diagnostic (San Antonio, TX, USA). Deoxynucleotide mix (dNTP), RNAase inhibitor, Taq enzyme and dNTP were from Takara Biotechnology (Dalian, China). M-MLV reverse transcriptase was from Promega Corp (Madison, WI, USA). Fura-2 AM and 5-(and-6)-chloromethyl-2',7'-dichlorodihydrofluorescein diacetate acetyl ester (CM-H_2DCFDA) were purchased from AAT Bioquest (Sunnyvale, CA, USA) or from Invitrogen (Oregon, USA). Rabbit anti-$p22^{phox}$, anti-NOX2, anti-$p67^{phox}$ and anti-Rac1/2 antibodies were from Abcam (Cambridge, UK). Rabbit anti-$p40^{phox}$ and goat anti-$p47^{phox}$ antibodies were from LifeSpan Biosciences (Seattle, WA, USA). HRP-conjugated goat anti-mouse IgG, HRP-conjugated goat anti-rabbit IgG, monoclonal mouse anti-β-actin, PVDF membrane and ECL Western blot kit were from Beijing Kangweishiji (Beijing, China). Rat IL-6 ELISA kit, recombinant mouse stem cell factor (SCF) and IL-3 were from Invitrogen (Camarillo, CA, USA). Rat LTC_4 ELISA kit was from Cayman Chemical (Ann Arbor, MI, USA).

Isolation of rat peritoneal mast cells

Rat peritoneal mast cells were obtained as reported[6] from rat of the Sprague-Dawley strain (200-400 g). The harvested ascites was centrifuged (100 g, 2×5 min), mast cells were readily identified by their large size, granular structure, and were re-suspended in Krebs-Ringer buffer before use.

Mast cell culture and IgE sensitization

RBL-2H3 cells obtained from Shanghai Institutes of Biological Sciences, Chinese Academy of Sciences were grown in minimal essential medium (MEM; Hyclone) supplemented with 10% FBS (Hyclone), 100 $U.ml^{-1}$ penicillin and 100 $\mu g.ml^{-1}$ streptomycin (GIBCO), in a humidified atmosphere with 5% CO_2 at 37°C. Mouse bone marrow-derived mast cells (BMMC) were prepared from femurs of 4- to 8-week-old ICR mice as reported[20]. Cells were cultured in RPMI 1640 (Hyclone)

supplemented with 10% fetal bovine serum (FBS) (Hyclone), 100 U.ml^{-1} penicillin and 100 μg.ml^{-1} streptomycin (GIBCO), rIL-3 (5 ng.mL^{-1}) and SCF (5 ng.mL^{-1}) in a humidified atmosphere with 5% CO_2 at 37°C. BMMC were grown for 4 - 6 weeks before use (> 95% mast cells).

For IgE sensitization, RBL-2H3 cells were plated on 100-mm culture dishes or in 6-well plates (cell density 10^6 cells / ml) and incubated with anti-DNP IgE (1 μg.mL^{-1}) at 37 °C overnight. Peritoneal mast cells and BMMC were sensitized with DNP-specific IgE at 100 ng.mL^{-1} for 2 hrs at 37°C.

Calcium measurements and UVA irradiation

Mast cell calcium concentration was measured as reported, either in a DeltaRam V-PMT-based system (for Figs. 1***A***, 2, 6***D,*** S3 in the present work) or a DeltaRam X - CCD-based system (for Figs. 1***B***, 1***C***) for individual or multiple cell measurements respectively[1,2,6]. Mast cells were loaded with Fura-2 AM (to a final concentration of 10 μM) in Krebs-Ringer buffer for 30 min at 37°C before attachment to the bottom cover-slip of a Sykes-Moore perfusion chamber. Perifused mast cells sensitized with anti-DNP IgE were stimulated with DNP-BSA to trigger calcium increases. Naïve mast cells (not treated with IgE) were irradiated with UVA. The in-system monochromator (DeltaRam V, PTI Inc., New Jersey, USA) was used as a UVA light source (alternating at 340 / 380 nm at 1 Hz). UVA light intensity was increased by changing monochromater slit width (both in and out) from 2 to 3 or 4 nm (with irradiance from 1.5, to 3.2 or 5.6 μW.cm^{-2} respectively; equivalent to 0.90, 1.92, 3.36 mJ.cm^{-2} in 10 min, and to 1.80, 3.84, 6.72 mJ.cm^{-2} in 20 min), with continued calcium monitoring at increased slit-width (note the decreased noise level). Basal calcium was measured with the slit-width set at 2 nm (which had no effect on basal calcium concentration), with excitation alternating between 340 nm / 380 nm and emission at > 510 nm. An LED UVA monochromatic light source (380 nm, Lamplic, Shenzhen, China) was also used, as an outside UVA source, to irradiate mast cells from above, with an irradiance of 80 μW.cm^{-2}.

Reverse transcription-PCR detection of NOX isoform and subunit expression

Total RNA was prepared using TRIzol reagent (Invitrogen). Total RNA (2 μg)

was reverse transcribed, the resultant cDNA subjected to polymerase chain reaction (PCR). Primer sequences and expected sizes of the PCR products are shown in Table 1. Cycle conditions were as follows: preheating at 94°C for 3 min, followed by 30 cycles of 94°C for 30 s, 55°C for 30 s, 72°C for 30 s, then extension at 72°C for 10 min. PCR products were separated by electrophoresis on 1.5% agarose gel and imaged under ultraviolet light after staining with ethidium bromide. The house-keeping gene GAPDH was used as internal control.

Immunocytochemical identification of NOX2 and subunits

RBL-2H3 or BMMC were seeded on cover-slips and cultured overnight. Freshly isolated rat peritoneal mast cells were attached to Cell-Tak-coated cover-slips. Mast cells were fixed in paraformaldehyde 4% then permeabilized in Triton X-100 (0.2%). Non-specific binding in permeabilized cells was blocked in normal goat or rabbit serum. Mast cells were then incubated with primary antibodies rabbit anti-gp91^{phox} (NOX2), anti-p22^{phox}, anti-p67^{phox}, anti-p40^{phox}, anti-Rac1/Rac2, or goat anti-p47^{phox} overnight at 4°C. After thorough wash, cells were incubated with secondary Cy5-conjugated goat anti-rabbit antibody or rabbit anti-goat (for p47^{phox}) IgG antibody. Cell nucleus was stained with Hoechst 33342. Fluorescence images were taken in a laser scanning confocal microscope (Zeiss LSM 510 META), under a 63 × / 1.40 oil objective.

Measurement of ROS Production

The production of intracellular ROS was measured using the ROS-sensitive fluorescent probe CM-H_2DCFDA. Mast cells (10^6.mL^{-1}) suspended in Hanks balanced salt solution (HBSS) were incubated with CM-H_2DCFDA (final concentration 5 μM) for 30 min, cells were then washed, re-suspended, and aliquoted at 150 μL per well. RBL-2H3 in the 96-well plate were placed in a microplate reader (Infinite® F200 PRO, TECAN), baseline fluorescence was measured (F_0) before irradiation with the LED UVA light source (80 μW.cm^{-2} for 2 min), DCFDA fluorescence intensity (F) was then measured at 2 min intervals for 20 min with excitation / emission wavelengths at 485 / 535 nm respectively. DCFDA fluorescence intensity after UVA irradiation was then subtracted with baseline cell fluorescence, all

data points was then expressed as net increase in fluorescence ($F-F_0$). In experiments shown in Fig. 6***C***, such net fluorescence increase was normalized to that of scramble control-treated mast cells (F/Fsc). For inhibitor experiments, RBL-2H3 cells were incubated with DPI or NAC for 30 min before CM-H_2DCFDA addition.

RNAi down regulation of NOX2 and subunit expression

Small interfering RNAs (siRNAs) and scramble controls were synthesized by Genema (Shanghai, China). Specific siRNA sequences are shown in Table 2. RBL-2H3 cells were grown in 6-well plates overnight at confluency of 50-70%. Mixed siRNA and transfection reagent X-tremeGENE-siRNA in Opti-MEM medium was diluted (1:10) in growth medium, to obtain a final siRNA concentration of 100 nM. RBL-2H3 cells were treated in this siRNA-containing medium for 6-8 hrs before further growth in normal medium for a total of 24 hrs. Cell mRNA was then extracted to measure gene knockdown level by quantitative PCR (Q-PCR) as follows.

Total RNA (100 ng) was reverse transcribed. The resultant cDNA was subjected to real-time PCR with SYBR Green mix (BioRad), in IQ5 (BioRad). Specific primer sets were as follows (listed from 5'-3'; forward and reverse, respectively): NOX2, AGCATCCATATCCGCATTG and CCACTAACATCACCACCTC; $p22^{phox}$, GAGCGGTGTGGACAGAAG and CAGCAGTAAGTGGAGGACAG; $p47^{phox}$, GAAGAAGCCAGAGACATACC and CTACGACATCCACCACATC. Reactions were performed in a volume of 20 µl containing primers (0.5 µM). The PCR protocol consisted of an initial de-naturation step at 95 °C for 5 min and 40-45 cycles of de-naturation (95°C for 30 s), annealing (50 °C for 30 s), and extension (72 °C for 20 s), melting curve analyses were performed from 65 to 95 ^{o}C (0.5 ^{o}C / 15 s). After completion of PCR, the copy number of the target genes was calculated by plotting fluorescence intensity against cycle numbers. The expression level of target genes was evaluated by the ratio of the target mRNA to that of GAPDH.

LTC_4 and IL-6 ELISA assays

Down-regulation of RBL-2H3 $gp91^{phox}$ (NOX2), $p22^{phox}$ or $p47^{phox}$ expression by siRNA was performed 24 hrs before UVA irradiation. LTC_4 and IL-6 in culture medium were measured by ELISA kits according to manufacturer's instructions.

Statistical analysis

Each experiment reported here has been done at least three times on different days, for peritoneal mast cells also from different animals. Data are expressed as mean ± SEM and plotted with SigmaPlot. To examine the differences between experimental groups, Student's *T* test was used, with $P < 0.05$ taken as statistically significant.

Results

IgE receptor activation induced calcium oscillations in mast cells

To activate or cross-link plasma membrane IgER, rat peritoneal mast cells, RBL-2H3 and BMMC were first sensitized with anti-DNP-BSA IgE as described in Methods. In IgE-sensitized mast cells IgE molecules were bound to mast cell plasma membrane. These cells were loaded with Fura-2 AM, perifused, the IgE molecules bound to mast cell surface were then cross-linked with antigen DNP-BSA at different concentrations (Fig. 1***A***-1***C***). Such cross-linking stretchs the plasma membrane to activate intracellular calcium increase. In control peritoneal mast cells without addition of any DNP-BSA, a steady baseline was observed (Fig. 1***Aa***). DNP-BSA at 10 $\mu g.L^{-1}$ initiated sparse calcium spikes (Fig. 1***Ab***). DNP-BSA at 30 $\mu g.L^{-1}$ produced regular baseline calcium oscillations (Fig. 1***Ac***). DNP-BSA at 100 $\mu g.L^{-1}$ resulted in plateau oscillations (Fig 1***Ad***), whereas DNP-BSA at 300 $\mu g.L^{-1}$ induced plateau oscillations which gradually decayed into a low steady plateau (Fig 1***Ae***). DNP-BSA (0.1-100 $\mu g.L^{-1}$) in IgE-sensitized RBL-2H3 produced similar concentration-dependent effects (Fig. 1***Ba***-***Be***). Senzitized RBL-2H3 showed steady baseline level calcium in the absence of any DNP-BSA addition (Fig. 1***Ba***). DNP-BSA 0.1 $\mu g.L^{-1}$ had little effect (Fig. 1***Bb***). DNP-BSA 1 $\mu g.L^{-1}$ triggered low amplitude low frequency calcium spikes, but with a rather long latency (Fig. 1***Bc***). DNP-BSA 10 $\mu g.L^{-1}$ produced in RBL-2H3 regular baseline calcium oscillations (Fig. ***1Bd***), whereas DNP-BSA 100 $\mu g.L^{-1}$ resulted in more robust calcium oscillations over an elevated plateau (Fig. 1***Be***). Sensitized BMMC without DNP-BSA crosslinking showed baseline calcium level (Fig. 1***Ca***), BMMC stimulated with DNP-BSA at 1-100 $\mu g.L^{-1}$ produced concentration-dependent calcium oscillations, with DNP-BSA 1 $\mu g.L^{-1}$ showing no effect (Fig. 1***Cb***). DNP-BSA 10 $\mu g.L^{-1}$ elicited sparse calcium spikes (Fig. 1***Cc***). DNP-BSA 30 $\mu g.L^{-1}$ induced regular baseline calcium oscillations (Fig. 1***Cd***) whereas DNP-BSA 100 $\mu g.L^{-1}$ triggered high frequency oscillations over an elevated plateau (Fig. 1***Ce***). These data indicate that in all three mast cell types, IgE receptor activation induced concentration-dependent generation of calcium oscillations.

UVA irradiation induced calcium oscillations in mast cells

UVA irradiation-induced calcium oscillations were reproduced in mast cells (Fig. 2***A***-2***C***). When the monochromater slit width was maintained at 2 nm, steady baseline calcium was observed (Fig. 2***Aa***). With monochromator slit width increased to 3 nm, sparse calcium oscillations were observed; once the oscillations occurred, the oscillations could be maintained at slit width 2 nm (Fig. 2***Ab***). With the monochromator slit width increased from 2 to 4 nm, calcium oscillations appeared with a shorter latency; calcium spikes were regular, and spike amplitude was enhanced; such oscillations could be maintained for a long time when slit width was switched to 3 nm (Fig. 2***Ac***).

Similar to freshly isolated peritoneal mast cells, UVA irradiation induced calcium oscillations in RBL-2H3 (Fig. 2***B***). Steady baseline calcium was observed at monochromator slit width of 2 nm (Fig. 2***Ba***). Calcium oscillations emerged when slit width was increased to 3 nm, which persisted when slit width was switched back to 2 nm (Fig. 2***Bb***). At slit width of 4 nm, the UVA-induced calcium spikes were regular with enhanced magnitude; those oscillatory spikes persisted when monochromater slit width was switched to 3 nm (Fig. 2***Bc***). Therefore UVA irradiance at $3.2\text{-}5.6\times10^{-6}$ $W.cm^{-2}$ was able to trigger calcium oscillations in RBL-2H3 (Fig. 2***Ba***-2***Bc***). Similar calcium increases were also found in BMMC. When monochromater slit width was maintained at 2 nm, a steady baseline calcium was seen (Fig. 2***Ca***). When the slit width was increased from 2 nm to 3 or 4 nm, calcium concentration increased, the latency for calcium increase was longer at slit width of 3 nm than at 4 nm (Fig. 2***Cb***-2***Cc***). In BMMC, calcium oscillatory patterns after UVA irradiation were less profound (than peritoneal and RBL-2H2 mast cells). Taken together, these data indicate that UVA induced similar irradiance-dependent calcium oscillations in all three mast cell types.

An external LED UVA source (380 nm) induced similar oscillatory calcium increases in RBL-2H3 (Fig. 2***D***). In these experiments, the monochromator slit was maintained at 2 nm, with steady baseline calcium. Brief irradiation from a LED source (80 $\mu W.cm^{-2}$ for 2 min) induced marked calcium oscillations (Fig. 2***D***).

Expression and subcellular localization of NOX isoform and subunit in mast cells

Although isolated peritoneal mast cells showed robust calcium oscillations after IgE cross-linking and UVA irradiation, peritoneal mast cell preparation is a mixture containing other cell types. Although this will not affect single cell measurements under the microscope, purified mast cells are needed to detect NOX isoform and subunit expression, to avoid contamination from other cell types. For such works RBL-2H3 was used.

Of rodent NOX isoforms (NOX1-4, DUOX1/2) and subunits ($p22^{phox}$, $p67^{phox}$, $p47^{phox}$, $p40^{phox}$, Rac1/2), RT-PCR experiments revealed high expression of $gp91^{phox}$ (NOX2), $p22^{phox}$, $p67^{phox}$, $p47^{phox}$, $p40^{phox}$, Rac1, Rac2, moderate expression of DUOX2 in RBL-2H3, but no expression of NOX1, NOX3, NOX4, NOXO1, NOXA1, or DUOX1; significant expression of each was found in the respective postitive control tissues or cells (colon, hepatocytes, brain, kidney, thyroid gland)(Fig. 3***A***). Colon, hepatocytes, brain, kidney and the thyroid were used as positive control tissues because they have been reported rather convincingly in the literature to express high levels of NOX1/NOXO1/NOXA1, NOX2/associated subunits, NOX3, NOX4, DUOX1/2 respectively and we have now confirmed such a consensus. The $gp91^{phox}$ (NOX2), $p22^{phox}$, $p67^{phox}$, $p47^{phox}$, $p40^{phox}$, Rac1, Rac2 were all expressed in hepatocyte (Fig. 3***A***). Semi-quantitative analysis of expression levels of NOX1-4, DUOX1/1, NOXO1, NOXA1, $p67^{phox}$, $p47^{phox}$, $p40^{phox}$, Rac1, Rac2 in RBL-2H3 and in positive control tissues are shown (Fig. 3***B***). The $gp91^{phox}$ (NOX2) was expressed at a ratio of about 10% GAPDH level in RBL-2H3, DUOX2 was just detectable at 1%, but $p22^{phox}$, $p67^{phox}$, $p47^{phox}$, $p40^{phox}$, Rac1, Rac2 all showed expression ratios of > 70% (normalized to GAPDH expression level) in RBL-2H3 (Fig. 3***B***). As expected, expression of NOX1, NOX2, NOX3, NOX4, NOXO1, NOXA1, DUOX1, $p67^{phox}$, $p47^{phox}$, $p40^{phox}$, Rac1, Rac2 was observed in the respective postitive control rat tissues colon, hepatocyte, brain, kidney, thyroid, thyroid, colon, colon, hepatocytes (Fig. 3***A,*** 3***B***). Interestingly, hepatocytes expressed significant amount of gp91phox (NOX2) and all associated subunits $p22^{phox}$, $p67^{phox}$, $p47^{phox}$, $p40^{phox}$, Rac1/2 (Fig. 3***A,*** 3***B***). The expression levels of $p22^{phox}$, $p67^{phox}$, $p47^{phox}$, $p40^{phox}$, Rac1/2 in RBL-2H3

were higher than in hepatocyte controls (Fig. 3***B***). NOX2 ($gp91^{phox}$) expression in RBL-2H3 was slightly lower than in hepatocytes (Fig. 3***B***).

The subcellular localization of $gp91^{phox}$ (NOX2) and subunits was examined by immunocytochemistry (Fig. 4). The catalytic subunit $gp91^{phox}$ (NOX2) and regulatory subunits $p22^{phox}$, $p67^{phox}$, $p47^{phox}$, $p40^{phox}$, Rac1/2 were readily detected in peritoneal mast cell (Fig. 4***Aa***-4***Af***). Mast cells were easily distinguished from other cell types by their granular structure (indicated by green arrows). NOX2 (Fig. 4***Aa***) and $p22^{phox}$ (Fig. 4***Ab***) were found concentrated in a ring around the cell nucleus, as well as $p67^{phox}$ (Fig. 4***Ac***), $p47^{phox}$ (Fig. 4***Ad***), $p40^{phox}$ (Fig. 4***Ae***), and Rac1/2 (Fig. 4***Af***). Note the lack of presence of NOX2 and subunits in the nucleus (Fig. 4***Aa***-4***Af***), and the lack of similar spatial distribution in non-mast cells (Fig. 4***Aa-Af***). Such profound difference was particularly well-demonstrated in the case of Rac1/2 due to their strong expression in non-mast cells (Fig. 4***Af***).

In RBL-2H3, $gp91^{phox}$ (NOX2)(Fig. 4***Ba***), $P22^{phox}$ (Fig. 4***Bb***), $p67^{phox}$ (Fig. 4***Bc***), $p47^{phox}$ (Fig. 4***Bd***), $p40^{phox}$ (Fig. 4***Be***), Rac1/2 (Fig. 4***Bf***) were all present in a ring around the nucleus, this region being wider than found in peritoneal mast cells (Fig. 4***Bc***-4***Bf***), but $P22^{phox}$ (Fig. 4***Bb***) and $p40^{phox}$ (Fig. 4***Be***) were also present in the nucleus. Note the particular puncta pattern and high nuclear to plasma ratio of $P22^{phox}$ (Fig. 4***Bb***), and low nulcear to plasma ratio of $p40^{phox}$ (Fig. 4***Be***).

Similar peri-nuclear presence of $gp91^{phox}$ (NOX2) was verified in BMMC (Fig. 4***Ca***), the presence of $p47^{phox}$ and Rac1/2 in BMMC were also found (Fig. 4***Cb, 4Cc***).

The above data together indicate that $gp91^{phox}$ (NOX2), $p22^{phox}$, $p67^{phox}$, $p47^{phox}$, $p40^{phox}$, Rac1, Rac2 were all expressed both at the mRNA and protein levels in all three mast cell types. Although DUOX2 mRNA was detected in RBL-2H3, DUOX2 protein was not detected by immunocytochemistry in either peritoneal mast cells or in RBL-2H3 (not shown), indicating that DUOX2 function may not be vitally important in mast cells.

Vital role for NOX2 in UVA irradiation-induced calcium oscillations, ROS and cytokine production in mast cells

CM-H_2DCFDA-loaded RBL-2H3 ($10^6.mL^{-1}$)(in 96-well plate) without UVA

irradiation showed a steady level of baseline ROS, but when irradiated with LED UVA (380 nm at 80 μW.cm^{-2}, for 2 min) generated significant amount of ROS (compared with control) (Fig. 5). UVA irradiation (from -2 min to 0 min) induced significant ROS production at min 2, which continued to increase, to reach a plateau level at min 8, and remained at this plateau level until the end of the experiment (Fig. 5). UVA irradiation-induced ROS production was blocked almost completely when RBL-2H3 were previously incubated with NOX inhibitor DPI (50 μM) or with antioxidant N-acetyl-cysteine (NAC, 2 mM) for 30 min (Fig. 5), but extracellular addition of catalase had no effect on intracellular ROS generation (Fig. S1). Further, UVA alone did not induce any ROS in the absence of RBL-2H3 cells (Fig. S1). These data indicated that both NOX activation and probably ROS was needed for maximal ROS production, suggesting a possible positive feedback loop.

The expression of gp91^{phox} (NOX2), p22^{phox}, p47^{phox} mRNA was down regulated by interfering RNA (siRNA). For such experiments, RBL-2H3 were incubated with specific siRNA at 100 nM (see Methods). Subsequent real-time quantitative PCR revealed that gp91^{phox} (NOX2), p22^{phox}, p47^{phox} mRNA expression was reduced to 33%, 11%, 23% of scramble controls ($P < 0.01$) (Fig. 6***A***). After such siRNA treatment, gp91^{phox} (NOX2), p22^{phox}, p47^{phox} protein expression in RBL-2H3, as assessed by Western blot, was decreased to (26.32 ± 3.56) %, (56.08 ± 7.10) %, (56.25 ± 4.56) % of scramble controls respectively ($P < 0.05$) (Fig. S2). Immunocytochemistry further confirmed down regulation of NOX2, p22^{phox} and p47^{phox} proteins in RBL-2H3. In scramble control-transfected RBL-2H3, NOX2, P22^{phox}, P47^{phox} were readily detected. NOX2 and P47^{phox} were present in the RBL-2H3 cell outside the nucleus, whereas P22^{phox} was found also in the nucleus in a puncta pattern, similar to that shown in untreated control RBL-2H3 cells seen in Fig. 4. But after specific siRNA treatment against NOX2, P22^{phox}, P47^{phox} expression, the fluorescence signal was markedly reduced in each case, further confirming that not only mRNA but also protein expression was down-regulated (Fig. 6***B***).

In RBL-2H3 cells where gp91^{phox} (NOX2), p22^{phox}, p47^{phox} expression was down-regulated by siRNA treatment, UVA irradiation-induced ROS generation was

reduced markedly in comparison with scramble controls (Fig. 6***C***). In these experiments, ROS production in scramble control cells were taken as 1, and ROS generation in specific siRNA-treated cells was normalized towards this reference point. Both baseline (time zero) and UVA-irradiation-induced ROS generation was reduced significantly after siRNA transfection of RBL-2H3 cells. The baseline ROS was (60.02 ± 0.02)%, (53.21 ± 0.21)%, and (79.04 ± 0.09)% of scramble control (Fig. 6***C***). UVA irradiation-induced ROS production was markedly reduced at all time points in siRNA-treated RBL-2H3 cells. At 6 min after UVA irradiation, for example, ROS production was reduced to (42.17 ± 0.17) % after siRNS-NOX2 treatment, whereas ROS production was reduced to (29.73 ± 0.15) % after siRNA-$P22^{phox}$ treatment, and ROS production was decreased to (28.11 ± 0.11) % of scramble control after siRNA-$P47^{phox}$ treatment (Fig. 6***C***). Such reduced ROS production was maintained until the end of the experiment (Fig. 6***C***).

In RBL-2H3 with siRNA-down regulated $gp91^{phox}$ (NOX2), $p22^{phox}$, or $p47^{phox}$ expression, UVA from either monochromator or LED source failed to induce significant calcium oscillations, whereas time-matched scramble control-treated RBL-2H3 still showed robust calcium oscillations after UVA irradiation (Fig. 6***D***). It was found that UVA irradiation of the scramble control-treated RBL-2H3 cells produced calcium oscillations at a slit width of 4 nm (Fig. 6***Da***-6***Dc***). But in RBL-2H3 cells whose expression of $gp91^{phox}$ (NOX2), $p22^{phox}$, $p47^{phox}$ was down-regulated by siRNA, UVA irradiation produced no obvious calcium oscillations (Fig. 6***Df***-6***Dh***). In the case of NOX2 or $p47^{phox}$ down regulation, some blunt fluctuations remained, but no calcium spikes occurred (compare Fig. 6***Da*** with 6***Df,*** Fig. 6***Dc*** with 6***Dh***). In the case of $p22^{phox}$ down regulation, a complete flat line was found (compare Fig. 6***Db*** with Fig. 6***Dg***). But in all cases no hallmark calcium spikes were found (Fig. 6***Df***-6***Dh***). Similarly, UVA irradiation from an LED source (380 nm at 80 $\mu W.cm^{-2}$) induced calcium oscillations in scramble control-treated RBL-2H3 (Fig. 6***Dd***, **6*De***), but after down regulation of NOX2 and $p47^{phox}$ expression, LED UVA irradiation produced only flat baseline calcium (Fig. 6***Di,*** 6***Dj***). Such NOX2 down-regulation experiments proved unambiguously the pivotal role for NOX2 in

UVA-induced ROS generation and calcium oscillations in RBL-2H3 mast cells. In sharp contrast, it may be noted, the addition of extracellular catalase (at 400 $U.mL^{-1}$) had no effect on UVA-induced calcium oscillations (Fig. S3).

In RBL-2H3 with siRNA-disrupted expression of $gp91^{phox}$ (NOX2), $p22^{phox}$, $p47^{phox}$ respectively, UVA irradiation (LED, 80 $\mu W.cm^{-2}$ for 2 min)-induced IL-6 and LTC_4 release was reduced significantly, in comparison with scramble controls (Fig. 6***Ea***, 6***Eb***). In scramble control-treated RBL-2H3 cells, UVA irradiation induced IL-6 release was increased from 1.00 ± 0.10 to 2.71 ± 0.17 (N = 3) (Fig. 6***Ea***). Such UVA stimulation was decreased to 1.94 ± 0.16, 1.31 ± 0.03, and 1.38 ± 0.19 after down-regulation of NOX2, $p22^{phox}$ and $p47^{phox}$ expression respectively (Fig. 6***Ea***). In scramble control-treated RBL-2H3 cells, UVA irradiation induced LTC_4 release was increased from 1.00 ± 0.04 to 3.65 ± 0.12 (N = 3) (Fig. 6***Ea***). Such UVA stimulation was reduced to 1.45 ± 0.27, 1.41 ± 0.37, and 1.24 ± 0.11 after down-regulation of NOX2, $p22^{phox}$ and $p47^{phox}$ expression with specific siRNA respectively (Fig. 6***Eb***). Comparatively, UVA irradiation-induced LTC_4 release was more susceptible to siRNA down regulation of NOX2, $p22^{phox}$, and $p47^{phox}$ than UVA irradiation-induced IL-6 release. This may reflect the fact that IL-6 was released after activation of nuclear gene expression, whereas LTC_4 was released after PLA2-mediated release of arachidonic acid from plasma membrane phospholipids.

Discussion

In the present work we have shown that UVA irradiation induced cytosolic calcium oscillations in fresh isolated peritoneal mast cells, cultured RBL-2H3 and mouse BMMC. UVA-triggered calcium oscillations were very similar to those triggered by IgE receptor (FcεRI) activation in all three types of mast cell. Reverse transcription-polymerase chain reaction revealed high level expression of $gp91^{phox}$ (NOX2), $p22^{phox}$, $p47^{phox}$, $p67^{phox}$, $p40^{phox}$, Rac1/2, moderate expression of DUOX2, but no expression of NOX1, 3, 4, DUOX1, NOXO1, and NOXA1 in RBL-2H3. Immunocytochemistry confirmed the subcellular distribution of $gp91^{phox}$ (NOX2), $p22^{phox}$, $p47^{phox}$, $p67^{phox}$, $p40^{phox}$, Rac1/2 in fresh isolated peritoneal mast cells, in RBL-2H3, of NOX2, $p47^{phox}$ and Rac1/2 in BMMC. UVA irradiation-induced ROS generation was blocked by NOX inhibitor DPI and antioxidant NAC in RBL-2H3. Down regulation by siRNA of $gp91^{phox}$ (NOX2), $p22^{phox}$, $p47^{phox}$ expression effectively suppressed UVA irradiation-induced calcium oscillations, ROS, IL-6 and LTC_4 production in RBL-2H3. All these indicate that NOX2 mediated UVA irradiation-induced calcium oscillations and other functional changes in mast cells.

In the present paper we have extended our previous work in the following respects. We have confirmed that other than the freshly isolated rat peritoneal mast cells, UVA irradiation (alternating at 340 / 380 nm) also triggered calcium oscillations in cultured rat mast cell line RBL-2H3 and in mouse bone marrow-derived mast cells. Further, we have extended our previous work in that an outside continuous UVA source (LED) at 380 nm was able to trigger calcium oscillations in RBL-2H3. Since both RBL-2H3 and BMMC are more or less homogenous, the complications associated with mixture peritoneal mast cell preparations are now overcome. The present work identified NOX2 as responsible for UVA-induced calcium oscillations therefore it would be interesting in the future to examine whether other isoforms especially the monomeric NOX5 when expressed ectopically in a non-NOX expressing cell line would result in calcium oscillations after UVA irradiation. In such future works, the exact location of the responsible UVA-absorbing and $^1O_2$-generating chromophore(s) within or without the NOX protein could be identified.

Activation of high affinity IgE receptor (FcεRI) in mast cell leads to the release of multiple pro-inflammatory mediators by degranulation, phospholipids metabolism, and by increased gene expression, to release histamine, proteases, arachidonate metabolites, chemotactic factors, and cytokines[21]. The mast cell-line RBL-2H3 has both mast cell and basophil characteristics, and shows typical FcεRI mediated signaling[22]. The FcεRI cross-linking or cell surface stretching triggered mast cell activation and calcium oscillations is a gold standard for testing mast cell function[23-25]. This typically involves an IgE-binding or sensitization step, and a subsequent antigen cross-linking step. In the present work, different concentrations of DNP-BSA were used to activate mast cell and calcium oscillations were seen in *all* three mast cell types: peritoneal mast cells, RBL-2H3 and BMMC (Fig. 1). DNP-BSA from 10-100 $\mu g.L^{-1}$ induced calcium oscillations, concentrations commonly used for stimulating mast cells (10-200 $\mu g.L^{-1}$)[5, 26-28].

As the major solar UV component on the surface of the earth, UVA is the most biologically relevant. UVA has typical immunomodulatory effects and mast cells are important in this process[9,12]. Exogenous photosensitizer plus high dose UVA de-granulate rat mast cells, low doses of UVA inhibit antigen or compound 48/80-induced mast cell degranulation[12,29,30]. Although UVA pre-treatment inhibits secretagogue-stimulated histamine release from human mast cell line HMC1 and from human skin mast cells[12,31,32], UVA at different doses (50 $kJ.m^{-2}$, 15 $J.cm^{-2}$) could trigger sizable histamine release from rat peritoneal and human skin mast cells respectively[12,33]. UVA irradiation induces a cation-selective non-inactivating ion current in RBL-2H3 or rat peritoneal mast cells[34]. We have found that low dose UVA irradiation activates *NOX*, sequentially to produce ROS, phospholipase C activation, and calcium oscillations in rat peritoneal mast cells[6]. In the present work, UVA irradiation from a monochromator (DeltaRam V, Photon Technology International Inc.) alternating at 340/380 nm induced similar calcium oscillations in peritoneal mast cells, RBL-2H3, and BMMC (Fig. 2***A***-2***C***), similar to an LED source (380 nm) in RBL-2H3 (Fig. 2***D***). The dose range required to do so was 3.2 and 5.6 $\mu W.cm^{-2}$ for the monochromater, and was 80 $\mu W.cm^{-2}$ for the LED. Such doses are similar to that

reported in the literature for histamine release from rat peritoneal mast cells (50 $J.m^{-2}$, [33]). It should be noted that in terms of latency, LED source induced faster response in the present work.

It has been proposed before that a major ROS source in non-phagocytic cell is NOX[35]. This source has been confirmed before in UVA-irradiated rat peritoneal mast cells[6]. The mast cell line RBL-2H3 mimicked peritoneal mast cells in UVA-induced ROS generation and calcium oscillations (Figs. 2, 5). In the present work RBL-2H3 was found to express highly $gp91^{phox}$ (NOX2), $p22^{phox}$, $p47^{phox}$ and $p67^{phox}$, Rac1, Rac2 and moderately DUOX2. The $gp91^{phox}$ (NOX2) and $p22^{phox}$, $p47^{phox}$ and $p67^{phox}$, Rac1/2 were all expressed outside the nucleus in peritoneal mast cells, RBL-2H3 and BMMC (Figs. 3, 4). The $p22^{phox}$ and $p40^{phox}$ were also conspicuous in the nucleus in RBL-2H3 (Fig. 4***B***). Reverse transcription-polymerase chain reaction detected low level DUOX2 mRNA in RBL-2H3, but DUOX2 immunocytochemistry revealed no detectable signal (not shown). The lack of DUOX2 protein instead of mRNA in mast cells could indicate that DUOX2 expression is regulated transcriptionally in RBL-2H3.

Besides the mast cell and the hepatocyte, other cell types also typically express NOX isoforms. Colon epithelial cells predominantly express NOX1 and associated subunits NOXO1 and NOXA1[36]. Pancreatic stellate cells express NOX1, NOX2, NOX4[37]. Differentiated 3T3-L1 adipocytes express NOX4, to mediate free fatty acid (palmitate)- and glucose-stimulated monocyte chemotactic factor gene expression[38]. Intracellular NOX4 expression in the thyrocyte may be associated with thyroid carcinogenesis or estrus cycling[39]. Human cardiac fibroblasts express NOX4 and NOX5 to mediate pathological cardiac fibroblast activation[40]. Both endothelial cells and keratinocytes express NOX1, NOX2, NOX4[41,42], whereas some authors found all NOX1-5 are present in human smooth muscle cell[43]. At least NOX1 activity is found in human lymphocytes[44]. DUOX2 is highly expressed in the thyroid, but also expressed in salivary glands, respiratory tract epithelial cells, uterus, and gallbladder[45,46]. Although only subunits $p22^{phox}$ and $p40^{phox}$ were found in the nucleus in RBL-2H3 (Fig. 3), human NOX1-5 have all been reported to be conspicuously

present in the nucleus of human vascular endothelial cells[43].

All NOX isoforms mediate ROS production[20,38,47]. LED UVA irradiation-induced ROS increase in RBL-2H3 mast cells (Fig. 5) shows a time profile similar to other cell types such as the keratinocyte[48]. UVA irradiation induced ROS production and calcium oscillations in RBL-2H3 were both completely blocked by antioxidant N-acetyl-cysteine and by NOX inhibitor diphenyleneiodonium chloride (DPI) (Fig. 5), similar to peritoneal mast cells[6]. Down regulated expression of NOX2, $p22^{phox}$, $p47^{phox}$ by siRNA (Fig. 6***A***, 6***B***) resulted in marked suppression of UVA irradiation-induced ROS generation (Fig. 6***C***), calcium oscillation (Fig. 6***D***), IL-6 and LTC_4 production (Fig. 6***E***).

Mast cell is a major source of allergic and inflammatory eicosanoids and cytokines[49,50]. UVA activated NOX2 to produce ROS, which could then activate phopholipase Cγ to induce calcium increases (Fig. 6***E***, and[6]). Increased calcium then activates cytosolic phospholipase A_2 (PLA_2) to mediate arachidonic acid release[26,51,52], eventually leading to LTC_4 synthesis and release via the 5-lipoxygenase pathway[26,53]. LTC_4 release could further activate mast cell LTC_4 autoreceptor in a positive feedback loop to intensify further LTC_4 release[54]. Increased calcium by activating transcription factors such as NF-κB induces IL-6 synthesis and release[21,22,55-57], in the present work probably with the following sequence of events: UVA – $^1O_2$ - NOX2 – ROS – PLCγ – calcium oscillations – [PLA2 activation – LTC4 / NF-κB – IL-6] (Fig. S4).

UV irradiation generally does not trigger calcium oscillations in other normal cell types. Other than the mast cell, the cancerous epithelial cell line HeLa has been reported to show calcium oscillations after UV irradiation, but at higher irradiance: 300 milliWatt.cm^{-2} (with un-specified UV spectrum range), but whether NOX is involved in UV-induced calcium oscillations in HeLa cells is not known[58]. Such difference in UV dosage indicates that it is much easier for UVA to induce calcium oscillations in mast cells, it could also mean that UVA-induced calcium oscillations in mast cells are probably more physiological, being associated with IL-6 / LTC_4 production (Fig. 6E), than in HeLa cells, where UV-induced calcium oscillations have been found to be associated with cell death[58].

In conclusion, NOX2 is identified in the present work to be the NOX isoenzyme responsible for UVA irradiation-induced ROS generation, triggeration of calcium oscillations and mediator production in mast cells. It will be interesting in the future to determine whether it is possible to reconstitute UVA-induced NOX2 production of ROS in a cell-free system, to determine whether and how $^1O_2$ is involved in UVA-induced NOX2 activation, and to clarify how ROS oxidatively activate the mast cell PLCγ to trigger calcium oscillations.

Acknowledgments: Work was supported by grants from NSFC (30970675, 31270892) and The MOST "973" Program (2011CB809101), and NSFBJ (5102020).

References

1 Y. J. Duan, H. Y. Liang, W. J. Jin and Z. J. Cui ZJ, Substance P conjugated to CdTe quantum dots triggers cytosolic calcium concentration oscillations and induces quantum dots internalization in the pancreatic carcinoma cell line AR4-2J, *Anal. Bioanal. Chem.*, 2011, **400**, 2995-3003.

2 H. Y. Liang HY, Z. M. Song and Z. J. Cui ZJ, Lasting inhibition of receptor-mediated calcium oscillations in pancreatic acini by neutrophil respiratory burst - a novel mechanism for secretory blockade in acute pancreatitis? *Biochem. Biophys. Res. Commun.,* 2013, **437**, 361-367.

3 B. J. Wang, H. Y. Liang and Z. J. Cui, Duck pancreatic acinar cell as a unique model for independent cholinergic stimulation-secretion coupling. *Cell. Mol. Neurobiol.* 2009, **29**, 747-756.

4 M. de Bernard, A. Cappon, L. Pancotto, P. Ruggiero, J. Rivera, G. Del Giudice and C. Montecucco, The *Helicobacter pylori* VacA cytotoxin activates RBL-2H3 cells by inducing cytosolic calcium oscillations. *Cell Microbiol.*, 2005, **l7**, 191-198.

5 M. M. Wilkes, J. D. Wilson, B. Baird and D. Holowka, Activation of Cdc42 is necessary for sustained oscillations of Ca^{2+} and PIP2 stimulated by antigen in RBL mast cells, *Biol. Open,* 2014: pii: BIO20148862, doi: 10.1242/bio.20148862.

6 Y. D. Zhou, X. F. Fang and Z. J. Cui, UVA-induced calcium oscillations in rat mast cells, *Cell Calcium*, 2009, **45**, 18-28.

7 R. M. Tyrrell, UVA (320-380 nm) radiation as an oxidative stress, *In*: Oxidative stress: oxidants and antioxidants, Pp 57-83, Academic Press, San Diego, 1991.

8 G. T. Wondrak, M. K. Jacobson and E. L. Jacobson, Endogenous UVA-photosensitizers: mediators of skin photodamage and novel targets for skin photoprotection, *Photochem. Photobiol. Sci.*, 2006, **5**, 215-237.

9 M. P. Stapelberg, R. B. Williams, S. N. Byrne and G. M. Halliday, The alternative complement pathway seems to be a UVA sensor that leads to systemic immunosuppression, *J. Invest. Dermatol.*, 2009, **129**, 2694-2701.

10 A. Hirota, Y. Kawachi, K. Itoh, Y. Nakamura, X. Xu, T. Banno, T. Takahashi, M. Yamamoto and F. Otsuka, Ultraviolet A irradiation induces NF-E2-related factor 2 activation in dermal fibroblasts: protective role in UVA-induced apoptosis, *J. Invest. Dermatol.*, 2005, **124**, 825-832.

11 M. Heckmann, M. Pirthauer and G. Plewig, Adhesion of leukocytes to dermal endothelial cells is induced after single-dose, but reduced after repeated doses of UVA, *J. Invest. Dermatol.*, 1997, **109**, 710-715.

12 S. Guhl, R. Stefaniak, M. Strathmann, M. Babina, H. Piazena, B. M. Henz and T. Zuberbier, Bivalent effect of UV light on human skin mast cells-low-level mediator release at baseline but potent suppression upon mast cell triggering, *J. Invest. Dermatol.*, 2005, **124**, 453-456.

13 J. Baier, T. Maisch, M. Maier, E. Engel, M. Landthaler and W. Bäumler, Singlet oxygen generation by UVA light exposure of endogenous photosensitizers, *Biophys. J.*, 2006, **91**, 1452-1459.

14 J. Baier, T. Maisch, M. Maier, M. Landthaler and W. Bäumler, Direct detection of singlet oxygen generated by UVA irradiation in human cells and skin, *J. Invest. Dermatol.*, 2007, **127**, 1498-1506.

15 W. Bäumler, J. Regensburger, A. Knak, A. Felgenträger and T. Maisch, UVA and endogenous photosensitizers - the detection of singlet oxygen by its luminescence, *Photochem. Photobiol. Sci.*, 2012, **11**, 107-117.

16 A. Knak, J. Regensburger, T. Maisch and W. Bäumler, Exposure of vitamins to UVB and UVA radiation generates singlet oxygen, *Photochem. Photobiol. Sci.*, 2014, **13**, 820-829.

17 S. D. Lamore, S. Azimian, D. Horn, B. L. Anglin, K. Uchida, C. M. Cabello and G. T. Wondrak, The malondialdehyde-derived fluorophore DHP-lysine is a potent sensitizer of UVA-induced photooxidative stress in human skin cells, *J. Photochem. Photobiol. B Biol.*, 2010, **101**, 251-264.

18 R. S. Sohal and R. Weindruch, Oxidative stress, caloric restriction, and aging, *Science*, **273**, 59-63.

19 G. Latouche, Z. G. Cerovic, F. Montagnini and I. Moya, Light-induced changes of

NADPH fluorescence in isolated chloroplasts: a spectral and fluorescence lifetime study. *Biochim. Biophys. Acta*, 2008, **1460**, 311-329.

20 T. Inoue, Y. Suzuki, T. Yoshimaru and C. Ra, Reactive oxygen species produced up- or downstream of calcium influx regulate proinflammatory mediator release from mast cells: role of NADPH oxidase and mitochondria, *Biochim. Biophys. Acta,* 2007, **1783**, 789-802.

21 A. M. Gilfillan and C. Tkaczyk, Integrated signalling pathways for mast-cell activation. *Nat. Rev. Immunol.*, 2006, **6**, 218-230.

22 T. Yoshimaru, Y. Suzuki, T. Inoue and C. Ra , L-type Ca^{2+} channels in mast cells: activation by membrane depolarization and distinct roles in regulating mediator release from store-operated Ca^{2+} channels, *Mol. Immunol.*, 2009, **l46**, 1267-1277.

23 T. Oka, K. Sato, M. Hori, H. Ozaki and H. Karaki, FcεRI cross-linking-induced actin assembly mediates calcium signalling in RBL-2H3 mast cells, *Br. J. Pharmacol.*, 2002, **136**, 837-846.

24 J. Narenjkar, S. J. Marsh and E. S. K. Assem, The characterization and quantification of antigen-induced Ca^{2+} oscillations in a rat basophilic leukaemia cell line (RBL-2H3), *Cell Calcium*, 1999, **26**, 261-269.

25 R. Cohen, A. Torres, H. T. Ma, D. Holowka and B. Baird, Ca^{2+} waves initiate antigen-stimulated Ca^{2+} responses in mast cells. *J. Immunol.*, 2009, **183**, 6478-6488.

26 Y. Lu, X. Li, Y. N. Park, O. Kwon, D. Piao, Y. C. Chang, C. H. Kim, E. Lee, J. K. Son and H. W. Chang, Britanin suppresses IgE/Ag-induced mast cell activation by inhibiting the Syk pathway, *Biomol. Ther. (Seoul)*, 2014, **22**, 193-199.

27 K. Seki, T. Hisada, T. Kawata, Y. Kamide, K. Dobashi, M. Yamada, M. Mori, F. Okajima and T. Ishizuka, Oxidative stress potentially enhances FcεRI-mediated leukotriene C4 release dependent on the late-phase increase of intracellular glutathione in mast cells, *Biochem. Biophys. Res. Commun.*, 2013, **439**: 357-362.

28 H. Subramanian, K. Gupta, N. Parameswaran and H. Ali, Regulation of FceRI

signaling in mast cells by G protein coupled receptor kinase-2 and its RH domain, *J. Biol. Chem.*, 2014, **289**, 20917-20927.

29 G. J. Gendimenico and I. E. Kochevar, Degranulation of mast cells and inhibition of the response to secretory agents by phototoxic compounds and ultraviolet radiation, *Toxicol. Appl. Pharmacol.*, 1984, **76**, 374-382.

30 J. Ring, B. Przybilla and B. Eberlein, Ultraviolet A inhibits histamine release from human peripheral leukocytes, *Intl. Arch. Allergy Appl. Immunol.*, 1989, **88**, 136-138.

31 C. Kronauer, B. Eberlein-Konig, J. Ring and H. Behrendt, Inhibition of histamine release of human basophils and mast cells *in vitro* by ultraviolet A (UVA) irradiation. *Inflamm. Res.*, 2001, **50(S2)**, S44-S46.

32 C. Kronauer, B. Eberlein-Konig, J. Ring and H. Behrendt, Influence of UVB, UVA and UVA1 irradiation on histamine release from human basophils and mastcells in vitro in the presence and absence of antioxidants, *Photochem. Photobiol.*, 2003, **77**, 531-534.

33 M. Mio, M. Yabuta and C. Kamei, Ultraviolet B (UVB) light-induced histamine release from rat peritoneal mast cells and its augmentation by certain phenothiazine compounds, *Immunopharmacology*, 1999, **41**, 55-63.

34 F. Mendez and R. Penner, Near-visible ultraviolet light induces a novel ubiquitous calcium-permeable cation current in mammalian cell lines. *J. Physiol.*, 1998, **507**, 365-377.

35 Y. Suzuki, T. Yoshimaru, T. Inoue, O. Niide and C. Ra, Role of oxidants in mast cell activation, *Chem. Immunol. Allergy*, 2005, **87**, 32-42.

36 M. Geiszt, K. Lekstrom, J. Witta and T. L. Leto, Proteins homologous to $p47^{phox}$ and $p67^{phox}$ support superoxide production by NAD(P)H oxidase 1 in colon epithelial cells, *J. Biol. Chem.*, 2003, **278**, 20006-20012.

37 A. Masamune, T. Watanabe, K. Kikuta, K. Satoh and T. Shimosegawa, NADPH oxidase plays a crucial role in the activation of pancreatic stellate cells, *Am. J. Physiol. Gastrointest. Liver Physiol.*, 2008, **294**, G99-G108.

38 C. Y. Han, T. Umemoto, M. Omer, L. J. D. Hartigh, T. Chiba, R. LeBoeuf, C. L.

Buller, I. R. Sweet, S. Pennathur, E. D. Abe and A. Chait, NADPH oxidase-derived reactive oxygen species increases expression of monocyte chemotactic factor genes in cultured adipocytes, *J. Biol. Chem.,* 2012, **287**, 10379-10393.

39 D. P. Carvalho and C. Dupuy, Role of the NADPH oxidases DUOX and NOX4 in thyroid oxidative stress, *Eur. Thyroid J.,* 2013, **2**, 160-167.

40 I. Cucoranu, R. Clempus, A. Dikalova, P. J. Phelan, S. Ariyan, S. Dikalov and D. Sorescu, NAD(P)H oxidase 4 mediates transforming growth factor-beta1-induced differentiation of cardiac fibroblasts into myofibroblasts, *Circ. Res.,* 2005, **97**, 900-907.

41 W. Chamulitrat, W. Stremmel, T. Kawahara, K. Rokutan, H. Fujii, K. Wingler, H. H. Schmidt and R. Schmidt, A constitutive NADPH oxidase-like system containing $gp91^{phox}$ homologs in human keratinocytes, *J. Invest. Dermatol.,* 2004, **122**, 1000-1009.

42 J. A. Sipkens, N. Hahn, C. S. van den Brand, C. Meischl, S. A. G. M. Cillessen, D. E. C. Smith, L. J. M. Juffermans, R. J. P. Musters, D. Roos, C. Jakobs, H. J. Blom, Y. M. Smulders, P. A. J. Krijnen, C. D. A. Stehouwer, J. A. Rauwerda, V. W. M. van Hinsbergh and H. W. M. Niessen, Homocysteine-induced apoptosis in endothelial cells coincides with nuclear NOX2 and peri-nuclear NOX4 activity, *Cell Biochem. Biophys.*, 2013, **67(SI2)**, 341-352.

43 L. Ahmarani, L. Avedanian, J. Al-Khoury, C. Perreault, D. Jacques and G. Bkaily, Whole-cell and nuclear NADPH oxidases levels and distribution in human endocardial endothelial, vascular smooth muscle, and vascular endothelial cells. *Can. J. Physiol. Pharmacol.*, 2013, **91**: 71-79.

44 M. Al-Essa, G. S. Dhaunsi, W. Al-Qabandi and I. Khan, Impaired NADPH oxidase activity in peripheral blood lymphocytes of galactosemia patients, *Exp. Biol. Med.* 2013, **238**, 779-786.

45 R. W. Harper, C. Xu, J. P. Eiserich, Y. Chen, C. Y. Kao, P. Thai, H. Setiadi and R. Wu, Differential regulation of dual NADPH oxidases/peroxidases, Duox1 and Duox2, by Th1 and Th2 cytokines in respiratory tract epithelium, *FEBS Lett.*,

2005, **579**, 4911-4917.

46 S. Morand, O. F. Dos Santos, R. Ohayon, J. Kaniewski, M. S. Noel-Hudson, A. Virion and C. Dupuy, Identification of a truncated dual oxidase 2 (DUOX2) messenger ribonucleic acid (mRNA) in two rat thyroid cell lines. Insulin and forskolin regulation of DUOX2 mRNA levels in FRTL-5 cells and porcine thyrocytes, *Endocrinology,* 2003, **144**, 567-574.

47 Q. Hu, Z. Yu, V. J. Ferrans, K. Takeda, K. Irani and R. C. Ziegelstein, Critical role of NADPH oxidase-derived reactive oxygen species in generating Ca^{2+} oscillations in human aortic endothelial cells stimulated by histamine, *J. Biol. Chem.* 2002, **227**, 32546-32551.

48 A. Valencia and I. E. Kochevar, Nox1-based NADPH oxidase is the major source of UVA-induced reactive oxygen species in human keratinocytes, *J. Invest. Dermatol.,* 2008, **128**, 214-222.

49 J. M. Brown, T. M. Wilson and D. D. Metcalfe, The mast cell and allergic diseases: role in pathogenesis and implications for therapy, *Clin. Exp. Allergy*, 2008, **38**, 4-18.

50 J. Kalesnikoff and S. J. Galli, New developments in mast cell biology, *Nat. Immunol.,* 2008, **9**, 1215-1223.

51 R. A. Dixon, R. E. Diehl, E. Opas, E. Rands, P. J. Vickers, J. F. Evans, J. W. Gillard and D. K. Miller, Requirement of a 5-lipoxygenase-activating protein for leukotriene biosynthesis, *Nature*, 1990, **343**, 282-284.

52 A. K. Mandal, J. Skoch, B. J. Bacskai, B. T. Hyman, P. Christmas, D. Miller, T. T. Yamin, S. Xu, D. Wisniewski, H. F. Evans and R. T. Soberman, The membrane organization of leukotriene synthesis, *Proc. Natl. Acad. Sci. U. S. A*, 2004, **101**, 6587–6592.

53 A. Zussman and R. Sagi-Eisenberg, Stimulation of Ca^{2+}-dependent exocytosis and release of arachidonic acid in cultured mast cells (RBL-2H3) by quercetin, *Intl. J. Immunopathol. Pharmacol*., 2000, **22**: 747-754.

54 J. Di Capite, C. Nelson, G.. Bates and A. B. Parekh, Targeting Ca^{2+} release-activated Ca^{2+} channels and leukotriene receptors provides a novel

combination strategy for treating nasal polyposis, *J. Allergy Clin. Immunol.*, 2009, **124**, 1014-1021.

55 H. J. Jeong, H. N. Koo, H. J. Na, M. S. Kim, S. H. Hong, J. W. Eom, K. S. Kim, T. Y. Shin and H. M. Kim, Inhibition of TNF-alpha and IL-6 production by Aucubin through blockade of NF-kappa B activation RBL-2H3 mast cells, *Cytokine,* 2002, **18**, 252-259.

56 K. Kandere-Grzybowska, R. Letourneau, D. Kempuraj, J. Donelan, S. Poplawski, W. Boucher, A. Athanassiou and T. C. Theoharides, IL-1 induces vesicular secretion of IL-6 without degranulation from human mast cells, *J. Immunol.* 2003, **171**, 4830-4836.

57 I. Ashmole, S. M. Duffy, M. L. Leyland and P. Bradding, Contribution of Orai(CRACM)1 and Orai(CRACM)2 channels in store-operated Ca^{2+} entry and mediator release in human lung mast cells, *PloS One*, 2013, **8**, e74895.

58 Y. Lao and D. C. Chang, Mobilization of Ca^{2+} from endoplasmic reticulum to mitochondria plays a positive role in the early stage of UV- or TNFalpha-induced apoptosis, *Biochem. Biophys. Res. Commun.* 2008, **373**, 42-47.

Figure legends

Figure 1. IgE receptor crosslinking triggered calcium oscillations in mast cells. Rat peritoneal mast cells (***A***), cultured RBL-2H3 (***B***), or mouse BMMC (***C***) were sensitized as described with anti-DNP IgE, loaded with Fura-2 AM, perifused, then at time indicated by the horizontal bars, DNP-BSA at indicated concentrations was added. (***A***): Isolated rat peritoneal mast cells sensitized with anti-DNP IgE at 100 ng.mL^{-1} for 2 hrs. DNP-BSA perifused at 0 (***a***)、10 (***b***)、30 (***c***)、100 (***d***)、300 μg.L^{-1} (***e***). (***B***): RBL-2H3 sensitized with anti-DNP IgE (1 μg.mL^{-1}) overnight. DNP-BSA perifused at 0 (***a***)、0.1 (***b***)、1 (***c***)、10 (***d***)、100 μg.L^{-1} (***e***). (***C***): BMMC sensitized with anti-DNP IgE at 100 ng.mL^{-1} for 2 hrs. DNP-BSA perifused at 0 (***a***)、1 (***b***)、10 (***c***)、30 (***d***)、100 μg.L^{-1} (***e***). Calcium measurements were done in the PMT-based system in (***A***), and in the CCD-based system in (***B***, ***C***). Calcium tracings in panel (***A***) each were obtained from one individual cell, tracings in panels (***B***) and (***C***) were obtained from several cells. All calcium tracings shown are representative of *N* (as indicated) independent experiments.

Figure 2. UVA irradiation induced calcium oscillations in mast cells. Fura-2-loaded rat peritoneal mast cells (***A***), cultured RBL-2H3 (***B***, ***D***), or mouse BMMC (***C***) were perifused, the monochromater slit-width was increased from 2 to 3 or 4 nm as indicated by the horizontal bars (***A-C***), or slit width was maintained at 2 nm but irradiated with an LED source (***D***). Calcium tracings in each panel (obtained from one individual cell in the PMT-based system) are representative of *N* (as indicated) independent experiments. UVA power for monochromater (alternating 340/380 nm) slit width 2, 3, 4 nm were 1.5, 3.2, 5.6 μW.cm^{-2} respectively. LED power was (380 nm, 80 μW.cm^{-2}).

Figure 3. RT-PCR detection of NOX mRNA expression in RBL-2H3. Mast cells and positive control tissues or cells were processed, RT-PCR products separated on 1% agarose gel and quantitated. Representative gel images of NOX isoform mRNA from RBL-2H3 and positive control tissues (colon, hepatocytes, brain, kidney, thyroid)

were presented (***A***), with GAPDH mRNA served as internal control. Data from 3 or 4 independent experiments were analyzed, normalized to that of GAPDH, and expressed as mean ± SEM (***B***). Note that representative original images shown in panel (***A***) were from 4 different experiments: (1) RBL-2H3 NOX2, $p22^{phox}$, $p67^{phox}$, $p47^{phox}$, $p40^{phox}$, Rac1, Rac2; (2) RBL-2H3 NOX1, NOX3, NOX4, DUOX1, DUOX2, NOXO1, NOXA1; (3) Hepatocyte NOX2, $p22^{phox}$, $p67^{phox}$, $p47^{phox}$, $p40^{phox}$, Rac1, Rac2; (4) Colon NOX1, NOXO1, NOXA1; Thyroid DUOX1, DUOX2; Brain NOX3; Kidney NOX4.

Figure 4. Immunocytochemical detection of NOX isoforms or subunits $gp91^{phox}$ (NOX2), $p22^{phox}$, $p67^{phox}$, $p47^{phox}$, $p40^{phox}$ Rac1/2 in mast cells. Rat peritoneal mast cells (***A***), RBL-2H3 (***B***), or mouse BMMC (***C***) were processed as described in Methods. Primary antibodies against NOX2 (***a***), $p22^{phox}$ (***b***), $p67^{phox}$ (***c***), $p47^{phox}$ (***d***), $p40^{phox}$ (***e***), Rac1/2 (***f***) in panels (***A***) and (***B***), against NOX2 (***a***), $p47^{phox}$ (***b***), Rac1/2 (***c***) in panel (***C***), Cy5-conjugated secondary antibody were used (red). Mast cell nucleus was stained with Hoechst 33342 (blue). In each panel (***A***-***C***) the first roll are merged fluorescence images and second roll merged fluorescence and bright field images. Arrows (green) in panel (***A***) indicate peritoneal mast cells. Confocal images were taken in a laser scanning confocal microscope (Zeiss 510 META), with the following excitation wavelengths: Cy5 at 633 nm, Hoechst 33342 at 405 nm.

Figure 5. UVA irradiation-induced ROS generation was blocked by NOX inhibitor DPI or by antioxidant NAC in RBL-2H3 cells. RBL-2H3 loaded with CM-H_2DCFDA were aliquoted to 96-well plate, placed in a microplate reader, baseline fluorescence (F0) measured, then irradiated with LED light (380 nm, 80 $\mu W.cm^{-2}$) for 2 min, DCFDA fluorescence then measured was subtracted with baseline level and plotted. Control cells were not irradiated with LED. In separate groups of mast cells, NOX inhibitor DPI (50 μM) or anti-oxidant NAC (2 mM) were added 30 min before UVA irradiation. DCFDA fluorescence intensity was presented as mean ± SEM, $N = 3$. Asterisk (*) indicates $P < 0.05$.

Figure 6. UVA irradiation-induced calcium oscillations, ROS and cytokine production in RBL-2H3 were inhibited after siRNA down-regulated expression of NOX2, $p22^{phox}$, or $p47^{phox}$. (***A***) Real-time polymerase chain reaction (PCR) detection of NOX2, $p22^{phox}$, or $p47^{phox}$ mRNA expression. SC: scramble control. Target gene expression was normalized to that of *GAPDH*. Asterisk (*) indicates $P < 0.05$. (***B***) Immunocytochemical detection of NOX2, $p22^{phox}$, $p47^{phox}$. SC: scramble control. Anti-NOX2, anti-$p22^{phox}$, anti-$p47^{phox}$ primary antibodies and Cy5-conjugated secondary antibody were used (red). Mast cell nucleus was stained with Hoechst 33342 (blue). Confocal images were taken in a laser scanning confocal microscope (Zeiss 510 Meta), with the following excitation wavelengths: Cy5 at 633 nm, Hoechst 33342 at 405 nm. (***C***) UVA-induced ROS generation. SC: scramble control. RBL-2H3 were loaded with CM-H_2DCFDA, and irradiated with an LED source (380 nm, 80 $\mu W.cm^{-2}$, 2 min). Fluorescence ratios (F/Fsc) were normalized to that of scramble controls and presented as mean ± SEM. Asterisk (*) indicates $P < 0.05$, $N = 3$. (***D***) UVA irradiation-induced calcium oscillations. RBL-2H3 treated with scramble control (***Da-De***) or target siRNA (***Df-Dj***) against NOX2, $p22^{phox}$ and $p47^{phox}$ were loaded with Fura-2 AM, perifused and then UVA irradiated as indicated by the horizontal bars, by a monochromater ***(Da-Dc***, ***Df-Dh)*** or by an LED source (***Dd***, ***De, Di***, ***Dj)***. Calcium tracings shown were obtained from a PMT-based calcium measurement system and each are representative of *N* independent experiments (*N* numbers as indicated). (***E***) UVA irradiation-induced IL-6 and LTC_4 production. At 24 hrs after transfection with siRNA, RBL-2H3 were irradiated with UVA (80 $\mu W.cm^{-2}$, 2 min) and grown for a further 24 hrs, medium IL-6 (***Ea***), LTC_4 (***Eb***) were measured by ELISA and presented as mean ± SEM. SC, scramble controls. Asterisk (*) indicates $P < 0.05$, $N = 3$.

Table 1
Sequence of PCR primers used to amplify NOX isoforms and subunits

Gene	Forward sequence	Reverse sequence	Product size (bp)
NOX2	ATGGAGGTGGGACAATACA	CAGACTTGAGAATGGAGGC	313
NOX1	ATGGCA TCCCTT TAC TCT GA	CATTGT CCCACATTGGTC TC	530
NOX3	TTTGGGCCCTGTGGTCTTGTATG	AGTCTCCTGAGGCTCGGATGTGT	264
NOX4	CCCTAGCAGGAGAACAAGA	AACAAGCCACCCGAAAC	372
DUOX1	ATACGAAGACAGCGTCATCCC	GCGGCACATAGTGAGCAAAA	392
DUOX2	ACCTGGTCTTCAAATCGTCC	CCACATTCTTGGTCATCCCT	387
$p22^{phox}$	TCTATTGTTGCAGGAGTGCTCATC T	TTG GTAGGTGGCTGCTTGATG	338
$p47^{phox}$	CCTTCATTCGCCACATCG	CATCATACCACCTGGGAGC	237
$P67^{phox}$	TAT TCC ACC ACC TCC TAA CTC	GCT GGGTAGCATCATAACTG	497
$P40^{phox}$	GGTCTGCGTGCTGATGGA	CCAGTTGGTAGTGTCCTCGTC	358
NOXO1	TCCAAGACACCCAGTATCAGC	CAGGCTATGAATGGCAAGG	464
NOXA1	ATCCCTGATGACCACAACTCG	TGGCACATTCCTCCATACACTC	435
Rac1	CCTGCCTGCTCATCAGTTAC	AATCGTGTCCTTATCATCCCT	329
Rac2	ATGGAGCCGTGGGCAAGA	TAGCGAGAAGCAGATGAGGAACA	211

Table 2
siRNA sequence

Target gene	siRNA sequence (5' to 3')
NOX2 (gp91^{phox})	CCUGGAAACUACCUAAGAUTT; AUCUUAGGUAGUUUCCAGGTT
	CCCAGAUGCAAGAAAGAAATT; UUUCUUUCUUGCAUCUGGGTT
	CCUCCUAUGACUUGGAAAUTT; AUUUCCAAGUCAUAGGAGGTT
p22^{phox}	ACUCUAUUGUUGCAGGAGUTT; ACUCCUGCAACAAUAGAGUTT
	GAGCGGUGUGGACAGAAGUTT; ACUUCUGUCCACACCGCUCTT
	GACUCCCAUUGAGCCUAAATT; UUUAGGCUCAAUGGGAGUCTT
p47^{phox}	CACCUCUUGAACUUCUUCATT; UGAAGAAGUUCAAGAGGUGTT
	CCAUCGAGGUCAUUCAUAATT; UUAUGAAUGACCUCGAUGGTT
	GCCAACACUAUGUGUACAUTT; AUGUACACAUAGUGUUGGCTT
scramble control	UUCUCCGAACGUGUCACGUTT; ACGUGACACGUUCGGAGAATT

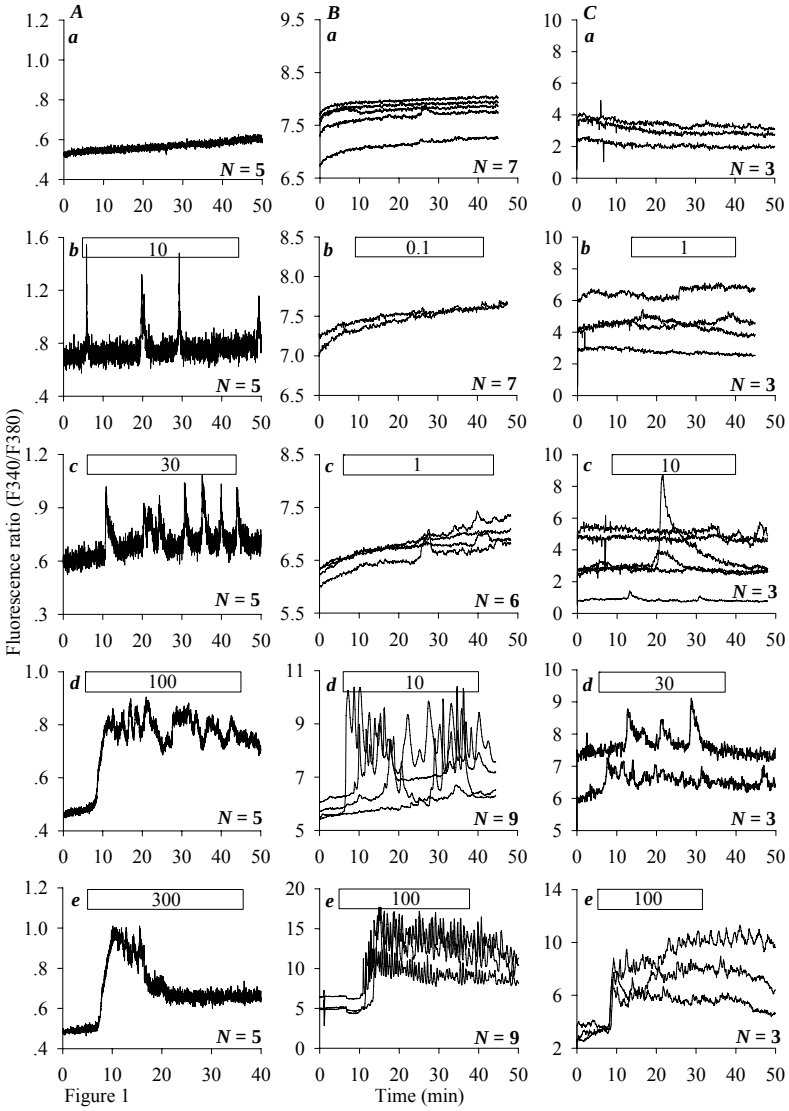

Figure 1

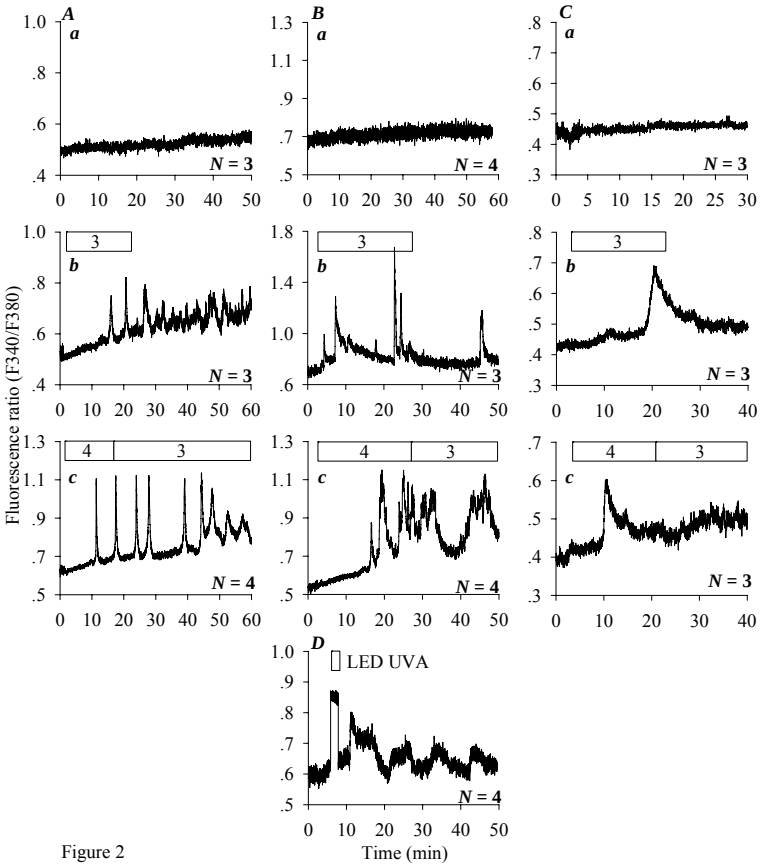

Figure 2

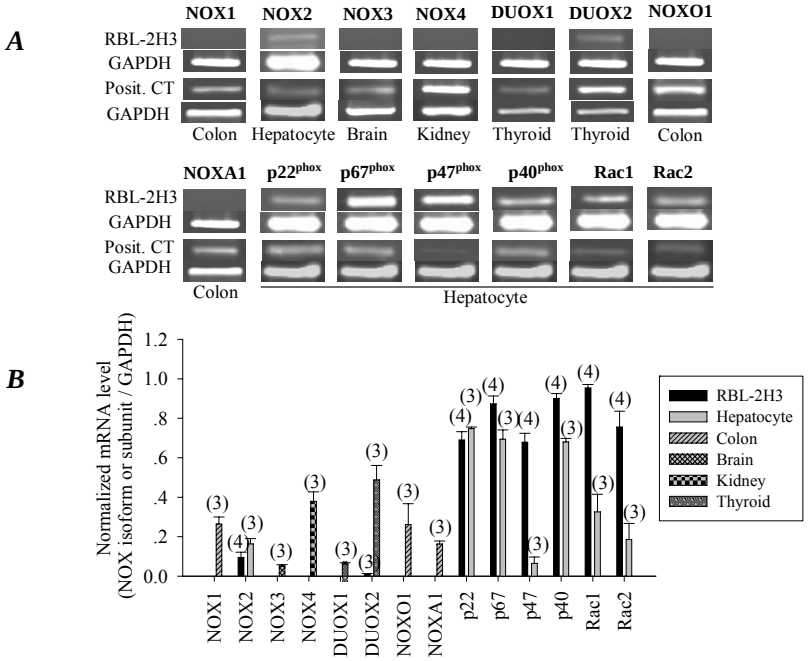

Figure 3

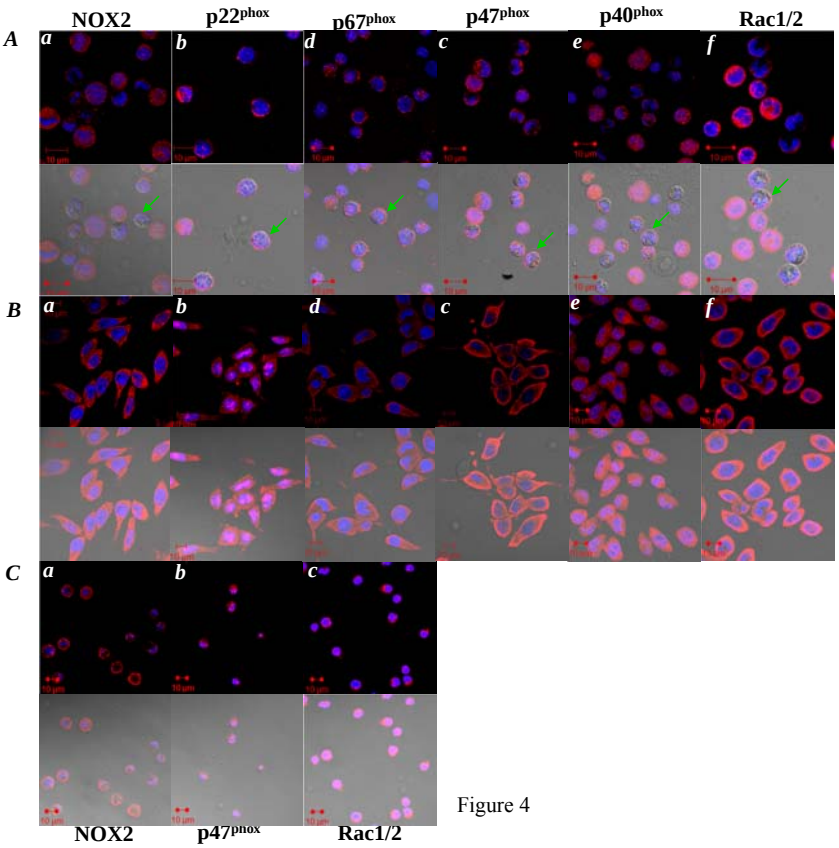

Figure 4

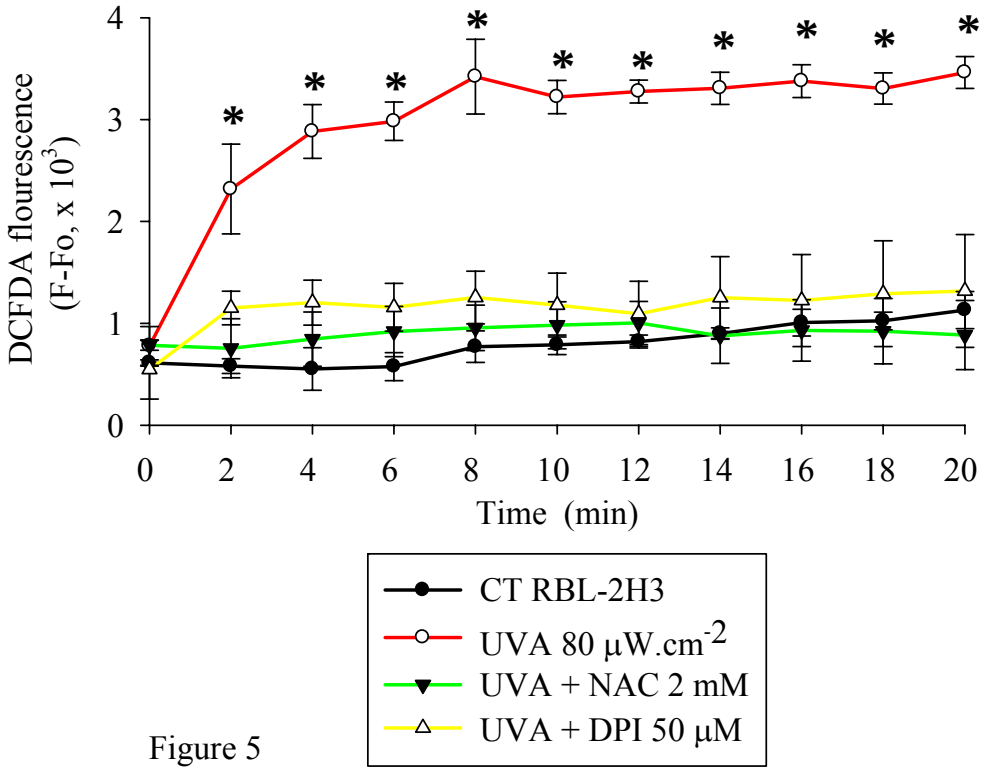

Figure 5

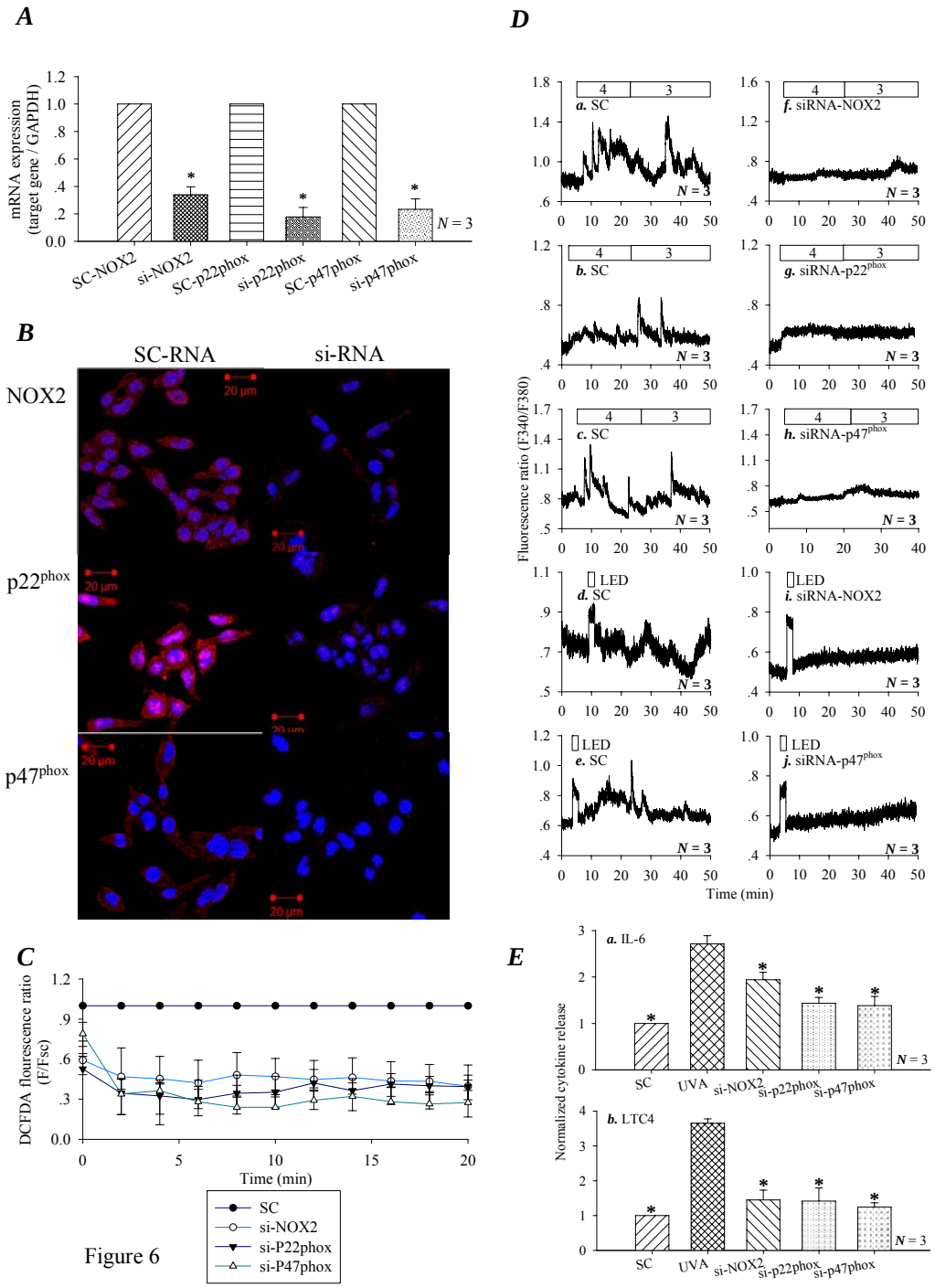

Figure 6